

# Efficient COVID-19 Detection using Optimized MobileNetV3-Small with SRGAN for Web Application

**Nattavut Sriwiboon**

Department of Computer Science and Information Technology, Faculty of Science and Health Technology, Kalasin University, Thailand  
nattavut.sr@ksu.ac.th

**Songgrod Phimphisan**

Department of Computer Science and Information Technology, Faculty of Science and Health Technology, Kalasin University, Thailand  
songgrod.ph@ksu.ac.th (corresponding author)

Received: 19 December 2024 | Revised: 19 January 2025 | Accepted: 24 January 2025

Licensed under a CC-BY 4.0 license | Copyright (c) by the authors | DOI: <https://doi.org/10.48084/etasr.9977>

## ABSTRACT

**Rapid and accurate detection of COVID-19 from medical images, such as X-rays and CT scans, is critical for timely diagnosis and treatment. This paper presents an innovative approach that combines Super-Resolution Generative Adversarial Network (SRGAN) for image enhancement with an optimized MobileNetV3-Small model to achieve efficient and high-accuracy classification. The proposed method significantly reduces computational complexity while maintaining performance. Specifically, the optimized MobileNetV3-Small model achieves 99.5% accuracy for X-ray images and 99.8% accuracy for CT images with only ~0.8M parameters and ~2.5 MB memory usage, making it highly suitable for real-time web applications in resource-constrained environments. Comparative analysis with related works demonstrates that the proposed approach outperforms other models in terms of accuracy, efficiency, and lightweight design. The results highlight the potential of the proposed method as a practical solution for rapid COVID-19 detection, contributing to the development of accessible and scalable diagnostic tools.**

*Keywords-COVID-19; SRGAN; MobileNetV3-Small; web application*

## I. INTRODUCTION

The global outbreak of COVID-19 has posed unprecedented challenges to healthcare systems worldwide, necessitating the development of rapid and accurate diagnostic tools. Medical imaging techniques, particularly X-rays and Computed Tomography (CT) scans, have proven to be invaluable in the early detection and monitoring of COVID-19 due to their non-invasive nature and accessibility. Deep learning, particularly Convolutional Neural Networks (CNNs) [1], has revolutionized the field of medical image analysis [2-4], enabling automated and accurate classification of diseases. Several studies [5-17] have focused on developing efficient, lightweight, and interpretable deep-learning models for COVID-19 detection and classification. However, existing models achieve high accuracy with large parameters, while lightweight models prioritize efficiency at the cost of performance.

This paper presents an enhanced approach that integrates advanced image enhancement techniques, using Super-Resolution Generative Adversarial Networks (SRGAN) [18],

with an optimized MobileNetV3 [19] architecture. The SRGAN is a deep learning model that enhances low-resolution images to high-resolution by combining a generator and a discriminator. The generator reconstructs high-resolution images, while the discriminator evaluates their realism. This adversarial training, guided by a perceptual loss function, enables SRGAN to produce high-quality photo-realistic images. The use of SRGAN improves the resolution and quality of X-ray and CT images, allowing CNN to extract features better. Subsequently, the optimized MobileNetV3-Small offers exceptional support for both X-ray and CT images, ensuring unmatched efficiency. Moreover, the lightweight design of the proposed model ensures compatibility with web-based applications, allowing for scalable and accessible deployment in real-world settings. The proposed model was evaluated on publicly available X-ray and CT image datasets, achieving performance comparable to existing models in terms of accuracy. By combining advanced image processing with a resource-efficient architecture, this study demonstrates the potential of deep learning-powered web applications to support rapid and reliable COVID-19 diagnosis. The contributions of this study are as follows:

- Employs SRGAN to enhance the resolution and quality of X-ray and CT scan images, improving feature visibility for accurate diagnosis.
- Develops an optimized MobileNetV3-Small [19] architecture, incorporating depthwise separable convolutions and simplified bottleneck layers to achieve low parameters and memory usage while maintaining high accuracy.
- Evaluates the model on publicly available datasets, demonstrating its performance in terms of accuracy for both X-ray and CT images compared to related works.
- The lightweight nature of the proposed model ensures efficient deployment in resource-constrained environments through a web application, providing real-time COVID-19 classification.
- Image enhancement with SRGAN: SRGAN is employed to enhance the resolution and quality of X-ray and CT images, making subtle features more distinguishable.
- Classification with optimized MobileNetV3-Small: A customized MobileNetV3-Small architecture is utilized for efficient feature extraction and accurate COVID-19 classification. The model is optimized to reduce parameters and memory while preserving performance.
- Web Application Deployment: The trained MobileNetV3-Small model is saved and integrated into a web application, enabling real-time COVID-19 detection in an accessible and scalable environment.

## II. THE PROPOSED METHODOLOGY

This section describes the proposed method for efficient COVID-19 detection using X-ray and CT images, focusing on a lightweight design for web-based deployment. Figure 1 illustrates the proposed model.

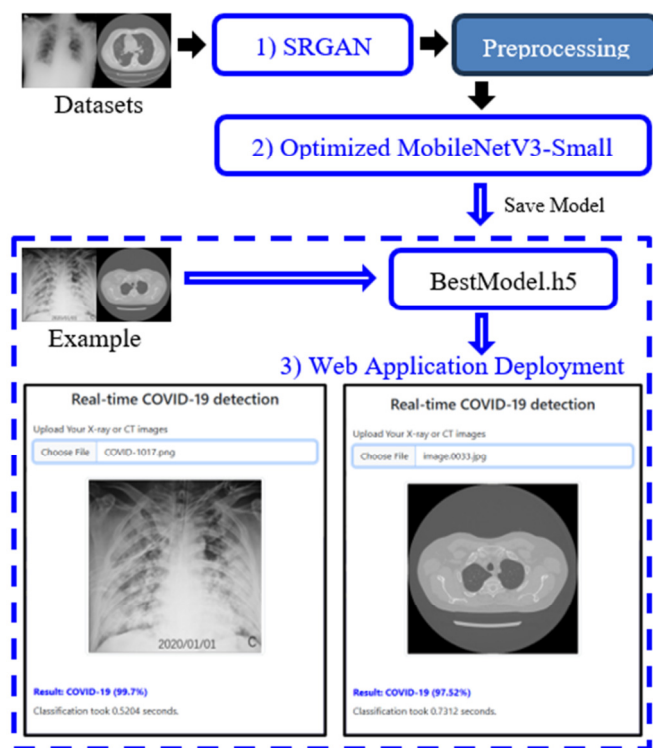


Fig. 1. The proposed model.

The proposed approach integrates advanced image enhancement techniques with a resource-efficient CNN architecture to achieve high accuracy while maintaining a low computational cost. The proposed method consists of three main components:

### A. Image Enhancement with SRGAN

SRGAN is integrated as a preprocessing step to improve the input quality for the CNN classifier. The proposed customized SRGAN leverages advanced image enhancement techniques to improve the resolution and quality of X-ray and CT images for efficient COVID-19 detection. The generator, with 16 residual blocks and an upscaling factor of 4, transforms low-resolution inputs  $64 \times 64$  into high-resolution outputs using pixel shuffle layers and ReLU activations, optimized with a learning rate of  $1e-4$  and the Adam optimizer. The discriminator, comprising 8 convolutional layers with Leaky ReLU activations, evaluates the realism of the generated images, guided by adversarial loss with a weight ( $\beta$ ) of  $1e-3$ . The total generator loss combines content loss (weighted  $\alpha = 1.0$ ), adversarial loss, and pixel loss (weighted  $\gamma = 1.0$ ) to ensure perceptual fidelity and pixel accuracy. The enhanced images are normalized and resized to  $224 \times 224$ . Figure 2(a) presents original images, while Figure 2(b) displays the results enhanced using SRGAN.

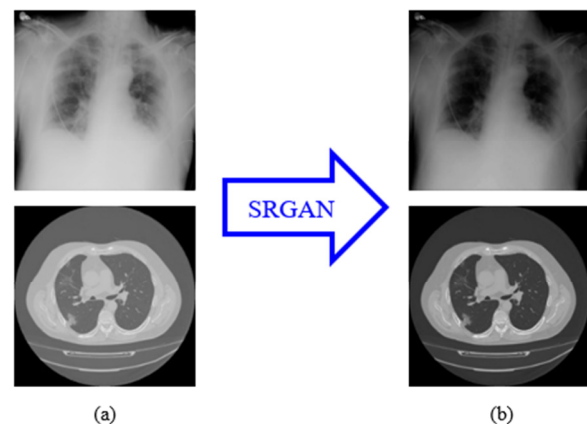


Fig. 2. (a) Original images, (b) images enhanced using SRGAN.

### B. Classification with Optimized MobileNetV3-Small

MobileNetV3 [19] utilizes depthwise separable convolutions, which decompose standard convolutions into depthwise and pointwise operations, significantly reducing computational costs. This design enables MobileNetV3-Small to maintain high accuracy with approximately 2.9 million parameters, requiring around 8 MB of memory, making it ideal for resource-constrained environments.

The proposed customized MobileNetV3-Small architecture incorporates key optimizations for a lightweight and efficient design. By extensively utilizing depthwise separable convolutions, the model reduces parameters and computational costs, splitting standard convolutions into per-channel filtering and pointwise operations. These enhancements ensure minimal resource usage while preserving high performance, as detailed in Table I. This reduces the number of parameters from  $K \times K \times C_{in} \times C_{out}$  to  $K \times K \times C_{in} + C_{in} \times C_{out}$ , ensuring high efficiency for resource-limited environments. Key modifications include the use of a compact  $3 \times 3$  convolution kernel to streamline feature extraction and bottleneck blocks optimized with a reduced expansion ratio of 4, significantly lowering the number of intermediate channels. The SE block is enhanced with an increased reduction ratio of 16, ensuring efficient recalibration of channel-wise feature maps without excessive computational cost. Additionally, the dense layer is simplified by reducing the number of neurons to 128, minimizing memory usage while preserving the effectiveness of the model.

TABLE I. PARAMETERS OF THE PROPOSED OPTIMIZED MOBILENETV3-SMALL

Layer Name	Type	Customized	Parameters (M)
Input Layer	Input	No	0.0
Conv2D	Convolution	Kernel size $K = 3 \times 3$	0.0043
Bottleneck block 1	Depthwise separable convolution	Reduced expansion ratio to 4	0.0768
Bottleneck block 2	Depthwise separable convolution	Reduced expansion ratio to 4	0.1284
Bottleneck block 3	Depthwise separable convolution	Reduced expansion ratio to 4	0.1920
SE blocks	Attention mechanism	Increased reduction ratio to 16	0.0400
Dense layer	Fully connected	Neurons reduced to 128	0.0737

As shown in Table I, by reducing the total parameters from approximately 2.9M in the original MobileNetV3-Small to ~0.8M (a reduction of 72.4%) and decreasing memory usage from 8 to ~2.5 MB (a reduction of 68.75%), the proposed model achieves a significant improvement in computational efficiency. These optimizations, which include depthwise separable convolutions, optimized SE blocks, hard-Swish activation, bottleneck refinements, and a simplified dense layer, allow the model to balance high accuracy with a lightweight design, making it ideal for real-time COVID-19 detection in resource-constrained environments such as web-based applications.

### III. EXPERIMENTS

#### A. Experimental Setup

The experiments were carried out using a system equipped with an Intel Core i7-9700K CPU running at 3.60GHz, an NVIDIA RTX 2080 Ti GPU with 11 GB memory, and 32 GB of RAM. The implementation utilized PyTorch 2.0 [20] as the deep learning framework, with the Adam optimizer ( $\beta_1 = 0.9$ ,  $\beta_2 = 0.999$ ) and a learning rate of  $1e - 4$ . The model was trained with a batch size of 50 epochs.

#### B. Datasets

The proposed model was evaluated on two publicly available datasets. The dataset introduced in [21] has publicly available X-ray images [22], with 12,576 categorized into COVID-19, normal, and pneumonia classes. The MosMedData [23] dataset includes 2,482 CT images labeled as COVID-19 and non-COVID cases. The datasets were split into 70% for training, 15% for validation, and 15% for testing to ensure a robust evaluation of the model's performance.

#### C. Preprocessing

X-ray and CT images were preprocessed using data augmentation techniques to improve robustness, including horizontal flipping (applied with a 50% probability), rotation (randomly selected angles within  $-15^\circ$  to  $+15^\circ$ ), and Gaussian noise injection ( $mean = 0$ ,  $variance = 0.01$ ). The images were preprocessed by resizing them to  $224 \times 224$  pixels and normalizing the pixel values to the range  $[0,1]$ , ensuring consistent input for the model while maintaining variability in the dataset to prevent overfitting.

#### D. Performance Metrics

The following metrics were used for the evaluation. Accuracy (Acc) [24] is a key metric for evaluating performance that indicates the proportion of correctly classified samples in the test dataset. To provide a holistic assessment of the model's effectiveness, additional metrics such as precision (PPV), sensitivity (Sen) [25], and F1-score (F1) [26] were considered. PPV measures the reliability of positive predictions, Sen assesses true positive detection, and F1 balances both, providing a comprehensive measure of the model.

$$Acc = \frac{TP+TN}{TP+FP+FN+TN} \quad (1)$$

$$PPV = \frac{TP}{TP+FP} \quad (2)$$

$$Sen = \frac{TP}{TP+FN} \quad (3)$$

$$F1 = 2 \cdot \frac{PPV \cdot Sen}{PPV + Sen} \quad (4)$$

## IV. RESULTS AND WEB APPLICATION

#### A. Results

The results of the evaluation demonstrate the progression of performance from the original MobileNetV3-Small to the proposed optimized MobileNetV3-Small, and finally to the SRGAN-enhanced optimized MobileNetV3-Small. The original MobileNetV3-Small, as shown in Table II, achieved 98.9% PPV, 99.1% Sen, 99.0% F1, and 99.0% Acc for X-ray images, and 99.2% PPV, 99.6% Sen, 99.4% F1, and 99.5% Acc for CT images. As shown in Table III, the optimized MobileNetV3-Small achieved 98.2% PPV, 98.7% Sen, 98.4% F1, and 98.5% Acc in X-ray images and 97.5% PPV, 98.2% Sen, 97.8% F1, and 98.0% Acc in CT images. As shown in Table IV, further enhancement using SRGAN resulted in exceptional performance, reaching 99.4% PPV, 99.6% Sen, 99.5% F1, and 99.5% Acc in X-ray images and 99.7% PPV, 99.8% Sen, 99.7% F1, and 99.8% Acc in CT images.

TABLE II. RESULTS OF ORIGINAL MOBILENETV3-SMALL

Metric	X-ray (%)	CT (%)
PPV	98.9	99.2
Sen	99.1	99.6
F1	99	99.4
Acc	99	99.5

TABLE III. RESULTS OF OPTIMIZED MOBILENETV3-SMALL

Metric	X-ray (%)	CT (%)
PPV	98.2	97.5
Sen	98.7	98.2
F1	98.4	97.8
Acc	98.5	98

TABLE IV. RESULTS OF SRGAN WITH OPTIMIZED MOBILENETV3-SMALL

Metric	X-ray (%)	CT (%)
PPV	99.4	99.7
Sen	99.6	99.8
F1	99.5	99.7
Acc	99.5	99.8

Although the original MobileNetV3-Small achieved strong performance, with 99% Acc in X-ray and 99.5% Acc in CT images, these results come at the cost of significantly higher parameters (2.9M) and memory usage (8 MB). The optimized MobileNetV3-Small achieved comparable results, with 98.5% Acc in X-ray and 98.0% Acc in CT images, while reducing the parameters to ~0.8M and memory to ~2.5 MB. This significant reduction in computational cost underscores the lightweight and resource-efficient design of the optimized MobileNetV3-Small, making it well-suited for real-time applications. Furthermore, the integration of SRGAN with the optimized MobileNetV3-Small further enhances performance, achieving 99.5% Acc in X-ray and 99.8% Acc in CT images. These results demonstrate that SRGAN not only compensates for the lightweight architecture but also elevates its performance beyond that of the original MobileNetV3-Small, making it a superior solution for COVID-19 detection in both X-ray and CT images.

### B. Web Application

The development of the web application for COVID-19 detection involves several steps and tools. Python served as the primary programming language, with TensorFlow/Keras [27] used to load and integrate the model for predictions. Flask [28] was employed to build the web application, creating routes for homepage display and prediction handling, while Numpy [29] and Pillow handled numerical computations and image preprocessing, including resizing to  $224 \times 224$  pixels and normalization to  $[0, 1]$ . The user interface was designed with HTML and CSS, offering a simple and intuitive platform for uploading X-ray and CT images and displaying predictions in real-time, as shown in Figure 3. This setup ensures a lightweight, efficient, and user-friendly solution for real-time COVID-19 detection in resource-constrained environments.

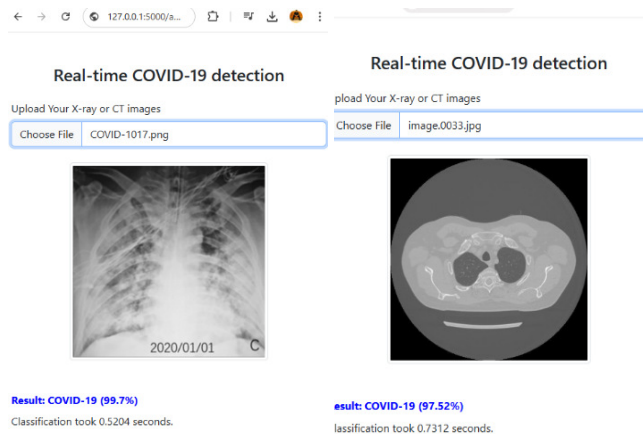


Fig. 3. Web application.

## V. DISCUSSION

The proposed optimized MobileNetV3-Small model with SRGAN was compared with existing methods, as shown in Table V. The comparative analysis reveals distinct differences in the application support and computational efficiency of the reviewed models, highlighting their strengths and limitations in handling X-ray and CT images, as well as their suitability for lightweight deployment.

FECNet [5] supports X-ray images exclusively, achieving accuracies of 92.70% (E1) and 92.53% (E2) with minimal computational requirements (~1M parameters and ~4 MB memory). Although lightweight, its lack of CT image support limits its applicability in broader medical diagnostics. SCNN [6] and LCCNN [7] focus exclusively on CT images, with SCNN achieving 94.88% accuracy using ~2.9M parameters and ~8 MB memory, and LCCNN achieving 91.78% accuracy with 1.9M parameters and ~7.76 MB memory. LCCNN is lighter but sacrifices accuracy, and both models lack support for X-ray images, restricting their versatility. DTL models [8] achieve a high accuracy of 98% on CT images but rely on computationally heavy architectures such as VGG16, requiring ~138M parameters and ~528 MB memory. These resource demands make these models unsuitable for lightweight, real-time applications. Similarly, BBO-CNN [9], designed for CT images, achieves moderate efficiency with 94.09% accuracy but requires ~5M parameters and ~20 MB memory, which is significantly less lightweight compared to modern optimized architectures. Multi-CNN models [10] broaden support to both X-ray and CT images, achieving 97% and 99% accuracy, respectively. However, their computational demands (~23M parameters and ~88 MB memory) hinder their deployment in resource-constrained environments. Despite their high accuracy, the lack of lightweight design limits their practicality for real-time use. RGFSAMNet [11], a strong competitor, supports both X-ray and CT images, delivering exceptional accuracy (99.48% for X-ray and 99.6% for CT). However, its resource-intensive nature (~25M parameters and ~100 MB memory) makes it unsuitable for lightweight applications, despite its high performance and explainability features.

In contrast, the proposed method that integrates SRGAN with Optimized MobileNetV3-Small offers comprehensive

support for both X-ray and CT images with unparalleled efficiency. The model achieves outstanding accuracies of 99.5% for X-ray and 99.8% for CT images, utilizing only ~0.8M parameters and ~2.5 MB memory. This lightweight design is significantly more efficient than all other reviewed models, enabling seamless deployment in real-time resource-

constrained environments such as web and mobile platforms. By combining versatility, high accuracy, and lightweight architecture, the proposed method sets a new benchmark for dual-modality COVID-19 detection, addressing the limitations of prior methods and making it the most practical and effective solution for modern diagnostic applications.

TABLE V. COMPARISON OF THE PROPOSED MODEL WITH RELATED WORKS.

Reference	Year	Dataset	Method	Best Acc.	Parameters	Memory	Application Support	
							X-ray Image	CT Image
[5]	2023	E1: 296 images, E2: 640	Four-Direction GLCM + ELM	92.70% (E1), 92.53% (E2)	~1M	~4 MB	✓	
[6]	2023	640 CT images	Swish-based CNN	94.88%	~2.9M	~8 MB	✓	
[7]	2023	640 CT images	Lightweight 8-layer CNN	91.78%	1.9M	~7.76 MB		✓
[8]	2023	2481 CT images	Transfer Learning (VGG16, ResNet-50, etc.)	98%	~138M	~528 MB	✓	
[9]	2024	296 CT images	BBO-CNN	94.09%	~5M	~20 MB		✓
[10]	2024	CT (746 images) + X-ray (2872 images)	Xception, ResNet-50, etc.	X-ray: 97%, CT: 99%	~23M	~88 MB	✓	
[11]	2024	CT (2482 images), X-ray (12,576 images)	ResNet-50 + Feature Fusion + Attention	X-ray: 99.48%, CT: 99.6%	~25M	~100 MB	✓	✓
Proposed		CT (2482 images), X-ray (12,576 images)	Optimized MobileNetV3-Small	X-ray: 98.5%, CT: 98%	~0.8M	~2.5 MB	✓	✓
			SRGAN with optimized MobileNetV3-Small	X-ray: 99.5%, CT: 99.8%				

## VI. CONCLUSION

This study presented a novel approach to COVID-19 detection by integrating SRGAN with an optimized MobileNetV3-Small model to effectively classify X-ray and CT images. The proposed method achieved outstanding accuracies of 99.5% for X-ray and 99.8% for CT images while significantly reducing computational complexity. By optimizing MobileNetV3-Small, a lightweight architecture with ~0.8M parameters and ~2.5 MB memory was achieved, making it a more efficient solution than existing works. Furthermore, SRGAN enhances image quality, allowing superior feature extraction and further improving classification performance. The proposed model addresses the limitations of existing methods, such as high computational demands, large parameter counts, and limited real-time applicability. Its ability to balance accuracy and efficiency ensures its suitability for deployment in resource-constrained environments, such as web-based and mobile applications, facilitating real-time COVID-19 detection.

Future work can explore further enhancements in image preprocessing, adaptive architecture tuning, and model generalization across larger and more diverse datasets. Overall, the proposed method provides a robust, lightweight, and high-performing solution for real-world COVID-19 diagnosis.

## REFERENCES

- [1] Y. Lecun, L. Bottou, Y. Bengio, and P. Haffner, "Gradient-based learning applied to document recognition," *Proceedings of the IEEE*, vol. 86, no. 11, pp. 2278–2324, Aug. 1998, <https://doi.org/10.1109/5.726791>.
- [2] S. T. Vemula, M. Sreevani, P. Rajarajeswari, K. Bhargavi, J. M. R. S. Tavares, and S. Alankritha, "Deep Learning Techniques for Lung Cancer Recognition," *Engineering, Technology & Applied Science Research*, vol. 14, no. 4, pp. 14916–14922, Aug. 2024, <https://doi.org/10.48084/etasr.7510>.
- [3] S. Khan, I. Ali, F. Ghaffar, and Q. Mazhar-ul-Haq, "Classification of Macromolecules Based on Amino Acid Sequences Using Deep Learning," *Engineering, Technology & Applied Science Research*, vol. 12, no. 6, pp. 9491–9495, Dec. 2022, <https://doi.org/10.48084/etasr.5230>.
- [4] S. Phimpisan and N. Sriwiboon, "A Customized CNN Architecture with CLAHE for Multi-Stage Diabetic Retinopathy Classification," *Engineering, Technology & Applied Science Research*, vol. 14, no. 6, pp. 18258–18263, Dec. 2024, <https://doi.org/10.48084/etasr.8932>.
- [5] Y. D. Zhang, V. Govindaraj, and Z. Zhu, "FECNet: a Neural Network and a Mobile App for COVID-19 Recognition," *Mobile Networks and Applications*, vol. 28, no. 5, pp. 1877–1890, Oct. 2023, <https://doi.org/10.1007/s11036-023-02140-8>.
- [6] Y. D. Zhang, Y. Pei, and J. M. Górriz, "SCNN: A Explainable Swish-based CNN and Mobile App for COVID-19 Diagnosis," *Mobile Networks and Applications*, vol. 28, no. 5, pp. 1936–1949, Oct. 2023, <https://doi.org/10.1007/s11036-023-02161-3>.
- [7] J. Wang, S. C. Satapathy, S. Wang, and Y. Zhang, "LCCNN: a Lightweight Customized CNN-Based Distance Education App for COVID-19 Recognition," *Mobile Networks and Applications*, vol. 28, no. 3, pp. 873–888, Jun. 2023, <https://doi.org/10.1007/s11036-023-02185-9>.
- [8] N. D. Kathamuthu *et al.*, "A deep transfer learning-based convolution neural network model for COVID-19 detection using computed tomography scan images for medical applications," *Advances in Engineering Software*, vol. 175, Jan. 2023, Art. no. 103317, <https://doi.org/10.1016/j.advengsoft.2022.103317>.
- [9] X. Han and Z. Hu, "Mobile Diagnosis of COVID-19 by Biogeography-based Optimization-guided CNN," *Mobile Networks and Applications*, Mar. 2024, <https://doi.org/10.1007/s11036-024-02301-3>.

- [10] N. Islam *et al.*, "COVID-19 and Pneumonia detection and web deployment from CT scan and X-ray images using deep learning," *PLOS ONE*, vol. 19, no. 7, 2024, Art. no. e0302413, <https://doi.org/10.1371/journal.pone.0302413>.
- [11] S. M. R. U. Karim, D. Bala, R. A. Rasul, and S. Goggins, "RGFSAMNet: An interpretable COVID-19 detection and classification by using the deep residual network with global feature fusion and attention mechanism." medRxiv, Nov. 01, 2024, <https://doi.org/10.1101/2024.10.30.24316451>.
- [12] K. Akyol, "ETSVF-COVID19: efficient two-stage voting framework for COVID-19 detection," *Neural Computing and Applications*, vol. 36, no. 29, pp. 18277–18295, Oct. 2024, <https://doi.org/10.1007/s00521-024-10150-0>.
- [13] G. M. Salama, A. Mohamed, and M. K. Abd-Ellah, "COVID-19 classification based on a deep learning and machine learning fusion technique using chest CT images," *Neural Computing and Applications*, vol. 36, no. 10, pp. 5347–5365, Apr. 2024, <https://doi.org/10.1007/s00521-023-09346-7>.
- [14] A. Utku and M. A. Akcayol, "Spread patterns of COVID-19 in European countries: hybrid deep learning model for prediction and transmission analysis," *Neural Computing and Applications*, vol. 36, no. 17, pp. 10201–10217, Jun. 2024, <https://doi.org/10.1007/s00521-024-09597-y>.
- [15] U. L. Marksia and C. Y. Rubavathi, "Accurate segmentation of COVID-19 infected regions in lung CT scans with deep learning," *Neural Computing and Applications*, vol. 36, no. 35, pp. 22511–22531, Dec. 2024, <https://doi.org/10.1007/s00521-024-10336-6>.
- [16] F. Altaf, S. M. S. Islam, and N. K. Janjua, "A novel augmented deep transfer learning for classification of COVID-19 and other thoracic diseases from X-rays," *Neural Computing and Applications*, vol. 33, no. 20, pp. 14037–14048, Oct. 2021, <https://doi.org/10.1007/s00521-021-06044-0>.
- [17] A. Paul, A. Basu, M. Mahmud, M. S. Kaiser, and R. Sarkar, "Inverted bell-curve-based ensemble of deep learning models for detection of COVID-19 from chest X-rays," *Neural Computing and Applications*, vol. 35, no. 22, pp. 16113–16127, Aug. 2023, <https://doi.org/10.1007/s00521-021-06737-6>.
- [18] C. Ledig *et al.*, "Photo-Realistic Single Image Super-Resolution Using a Generative Adversarial Network," in *2017 IEEE Conference on Computer Vision and Pattern Recognition (CVPR)*, Honolulu, HI, USA, Jul. 2017, pp. 105–114, <https://doi.org/10.1109/CVPR.2017.19>.
- [19] A. Howard *et al.*, "Searching for MobileNetV3," in *2019 IEEE/CVF International Conference on Computer Vision (ICCV)*, Seoul, Korea (South), Oct. 2019, pp. 1314–1324, <https://doi.org/10.1109/ICCV.2019.00140>.
- [20] A. Paszke *et al.*, "PyTorch: An Imperative Style, High-Performance Deep Learning Library," in *Advances in Neural Information Processing Systems*, 2019, vol. 32.
- [21] M. E. H. Chowdhury *et al.*, "Can AI Help in Screening Viral and COVID-19 Pneumonia?," *IEEE Access*, vol. 8, pp. 132665–132676, 2020, <https://doi.org/10.1109/ACCESS.2020.3010287>.
- [22] T. Rahman, M. Chowdhury, and A. Khandakar, "COVID-19 Radiography Database." Kaggle, 2020, [Online]. Available: <https://www.kaggle.com/datasets/tawsifurrahman/covid19-radiography-database>.
- [23] S. P. Morozov *et al.*, "MosMedData: Chest CT Scans With COVID-19 Related Findings Dataset." arXiv, May 13, 2020, <https://doi.org/10.48550/arXiv.2005.06465>.
- [24] W. J. Krzanowski and D. J. Hand, *ROC Curves for Continuous Data*. New York, NY, USA: Chapman and Hall/CRC, 2009.
- [25] A. G. Lalkhen and A. McCluskey, "Clinical tests: sensitivity and specificity," *Continuing Education in Anaesthesia Critical Care & Pain*, vol. 8, no. 6, pp. 221–223, Dec. 2008, <https://doi.org/10.1093/bjaceaccp/mkn041>.
- [26] J. Han, J. Pei, and H. Tong, *Data Mining: Concepts and Techniques*. Morgan Kaufmann, 2022.
- [27] M. Abadi *et al.*, "TensorFlow: Large-Scale Machine Learning on Heterogeneous Distributed Systems." arXiv, Mar. 16, 2016, <https://doi.org/10.48550/arXiv.1603.04467>.
- [28] M. Grinberg, *Flask Web Development: Developing Web Applications with Python*, 2nd ed. O'Reilly Media, 2018.
- [29] C. R. Harris *et al.*, "Array programming with NumPy," *Nature*, vol. 585, no. 7825, pp. 357–362, Sep. 2020, <https://doi.org/10.1038/s41586-020-2649-2>.